JPhys Photonics

PAPER • OPEN ACCESS

Impact of H_2 gas on disruptive birefringence optical fibers with embedded Palladium particles for developing robust sensors

To cite this article: Mohamed Aazi *et al* 2020 *J. Phys. Photonics* **2** 014005

JPhys Photonics

PAPER

Impact of H_2 gas on disruptive birefringence optical fibers with embedded Palladium particles for developing robust sensors

Mohamed Aazi[1,2], **Maryna Kudinova**[1], **Damien Kinet**[2], **Jean-Louis Auguste**[1], **Sylvie Delépine-Lesoille**[3], **Patrice Mégret**[2] **and Georges Humbert**[1]

[1] XLIM Research Institute, UMR 7252 CNRS/Limoges University, 123 av. A. Thomas, Limoges, France
[2] Electromagnetism and Telecommunication Department, Faculty of Engineering, University of Mons, Boulevard Dolez 31, B-7000 Mons, Belgium
[3] Andra, French National Radioactive Waste Management Agency, Parc de la Croix Blanche, 1-7 rue J. °Monnet, Chatenay- Malabry, France

E-mail: georges.humbert@xlim.fr

Keywords: optical fiber sensor, hydrogen, birefringence

OPEN ACCESS

RECEIVED
26 July 2019

REVISED
28 October 2019

ACCEPTED FOR PUBLICATION
28 November 2019

PUBLISHED
20 December 2019

Abstract

Optical fiber sensors of hydrogen gas (H_2) are conventionally based on the reaction of a sensitive material deposited on the surface of a fiber. Long-term applications of H_2 monitoring require more robust configurations, less sensitive to the degradations of the sensitive layer. To overcome this issue, we develop disruptive polarisation-maintaining optical fibers composed of a sensitive material (Palladium, Pd) integrated into the silica cladding. We present the development of two Panda-type optical fibers with or without embedded Pd particles. These fibers have been fabricated for evaluating, through the measurement of the birefringence, the contribution of Pd particles on the detection of H_2 gas. We have specially developed a gas chamber for measuring on-line the detection of H_2 during its diffusion into the fiber. Dynamic comparisons between both fibers demonstrate the contribution of Pd particles resulting in a faster response time (of about 20 h for our experimental conditions). These results pave the way to the realization of robust optical fibers with enhanced sensitivity to H_2 gas for developing sensing systems compatible with long-term hydrogen monitoring applications in extreme and harsh environments, such as radioactive waste repositories.

1. Introduction

It is well known that hydrogen is an explosive gas at low concentrations in air (from 4% to 75% Vol) [1]. Its detection and monitoring is thus crucial in many applications such as fuel cells, geothermal wells, nuclear power plants, radioactive waste storage or repository centers.

Conventional hydrogen sensors are developed to detect H_2 leaks, using a sensitive material such as tin oxide, tungsten oxide, platinum or palladium, whose resistive behavior and physicochemical properties are modified in contact with H_2 [2–9]. The direct contact between the sensitive material and H_2 enables fast response time, in the order of few seconds [10]. Optical fiber sensors are able to detect H_2 under harsh and explosive conditions, however, most fiber optic sensors are based on a deposit of a thin layer of sensitive material on the surface of the fiber. This configuration limits the sensor robustness and causes stability issues related to the degradation of the film after several exposure cycles [11]. To overcome this problem, we propose an optical fiber composed of a sensitive material (Palladium, Pd) integrated into the silica cladding in order to protect the sensing metal from harsh environments. Even if the response time will be in the order of hours, this technique would be ideal for long-term applications such as for monitoring slow H_2 release in radioactive wastes repositories. In these repositories, the releases of H_2 are very small and the kinetic is very slow. The evolution of H_2 concentration should be measured during decades with a measurement every week [12].

The detection of H_2 is expected to be realized by exploiting the mechanical strain induced by the crystal lattice expansion of Pd particles in contact with H_2 gas, which one affects the optical properties of the propagated light through the elasto-optic effect. In this purpose, we have already demonstrated the fabrication of an optical fiber with Pd particles embedded in the cladding, but without H_2 sensing tests [13]. In order to realize efficient fiber transducers for H_2 sensing, it is of primary importance to evaluate the contribution of Pd particles embedded into an optical fiber, for the detection of H_2. In this prospect, we report the first experimental comparison of H_2 sensors based on specialty optical fibers with or without embedded Pd particles. To realize this study we have fabricated high birefringence fibers (i.e. polarization maintaining (PM) fibers) by introducing two stress applying parts (SAP, opposite to each other on the side of the core) that give rise to stress fields in the fiber leading through the elasto-optic effect to an anisotropy of the refractive index in the core region (i.e. birefringence). The contribution of Pd particles have been studied by measuring and comparing the evolution of the birefringence of these fibers (with or without Pd particles inserted into the SAP materials) placed within a gas chamber filled with H_2 gas. The fabrication of the fibers, the experimental setup and the experimental results and their analyzes are presented in the following sections.

2. Fabrication of disruptive birefringent optical fibers

We have fabricated a PANDA-type birefringent optical fiber composed of two SAPs of glass material in which Pd particles are integrated. To fabricate the SAPs, we have used a glass material composed of $70SiO_2$–$20Al_2O_3$–$10La_2O_3$% mol (SAL). This SAL glass has a coefficient of thermal expansion ($\sim 5.3 \times 10^{-6}\,K^{-1}$) ten times higher than the silica one ($\sim 0.54 \times 10^{-6}\,K^{-1}$) that generates a significant mechanical stress in the fiber [14].

The SAL glass was elaborated with the conventional melt-quenching technique to form a bulk sample (figure 1(a)). The sample was then milled to a powder with a median diameter of particles about 15 μm. Palladium oxide (PdO) powder was then mixed with the SAL powder to form the material of the SAPs. The preform of the fiber was fabricated with the Modified Powder in Tube technique (MPIT) [15] associated with stack-and-draw process. As illustrated in figure 1(b), the preform was realized by surrounding a Germanium-doped silica rod with pure silica rods to form the fiber cladding. In order to form the SAPs, two silica tubes placed opposite to each other on the side of the fiber core were filled with the powder material (SAL and PdO). The core of the fiber is similar to the one of a standard single mode fiber (SMF). It was realized by using a Germanium-doped silica rod from a preform of an SMF. The preform was then heat-treated under specific conditions to reduce PdO to metallic Pd particles (figure 1(c)) [13].

In order to evaluate the contribution of Pd particles embedded into the SAPs, we have fabricated the same fiber preform without Pd particles in the SAPs, for obtaining a reference fiber that is named 'SAL-fiber' in the following. The preforms were drawn down to optical fibers with a drawing fiber tower. The scanning electron microscope (SEM) picture of the cross section of the SAL-fiber and of the fiber with Pd particles (named SALP-fiber) are shown in figures 2(a) and (b), respectively. Both fibers are composed of a Ge-doped core with a diameter of about 8 μm for ensuring single mode propagation in the spectral region around 1.55 μm. The diameter of the SAPs is about 24 μm and 21 μm for the SAL-fiber and SALP-fiber, respectively. It is worth noticing that the larger refractive index of SAL glass (than the silica one) requires to optically isolate the core and the SAPs by separating them by about 20 μm.

X-ray powder diffraction (XRD) was performed on the SAPs of the SALP-fiber for estimating the oxidation state of Pd particles. As shown in figure 2(c), the diffraction peaks match with the database patterns of Pd (JCPDS n°46-1043) proving the reduction of PdO particles [13]. This measurement demonstrates the fabrication of an optical fiber with Pd particles embedded in the SAPs.

3. Experimental setup and methods

3.1. Birefringence measurements

We used the high birefringence fiber loop mirror (FLM) configuration for measuring the birefringence of the PM fiber. As illustrated in the schematic of the figure 3(a), this setup is composed of a sample of the PM fiber under-test, 3 dB fiber-coupler, an optical spectrum analyzer (OSA), and an optical broadband source. The incident light is splitted by the 3 dB coupler into two counter propagating beams that are recombined after propagating throughout the PM fiber. The birefringence of the PM fiber induces a phase difference between the two orthogonal beams that leads to an interference spectrum at the output of the FLM [16, 17]:

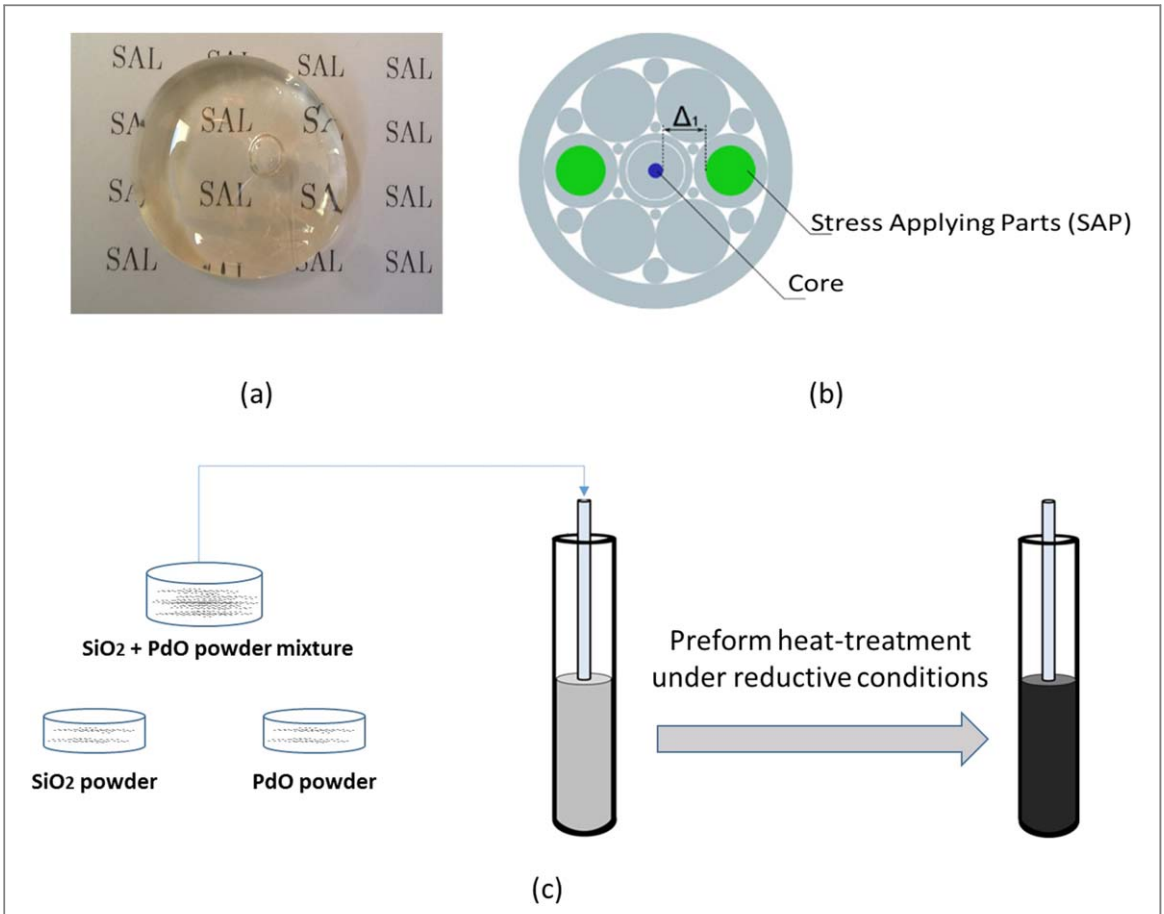

Figure 1. (a) Photograph of a bulk sample of SAL glass, (b) scheme of the fiber preform associating stack-and-draw and modified powder-in-tube technologies. The distance between the core and the SAP is noted Δ_1, (c) illustration of the MPIT based process developed for fabricating preforms with Pd particles embedded into the cladding material.

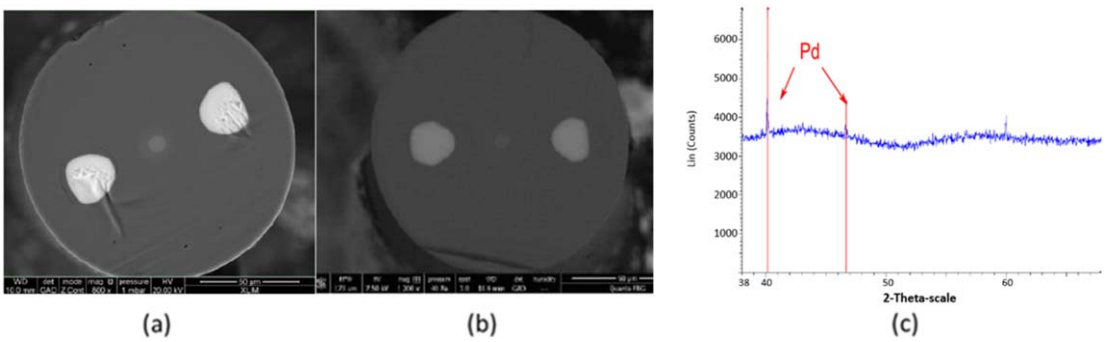

Figure 2. SEM (in the backscattered configuration) images of cross-sections of optical fibers fabricated by the MPIT process: (a) SAL fiber, (b) SALP fiber. (c) XRD diagram of Pd-based fiber of a heat-treated preform sample.

$$T(\lambda) = \left(\sin \frac{\pi BL}{\lambda}\right)^2, \tag{1}$$

where B is the fiber birefringence and L the fiber length.

This configuration presents many advantages such as a low sensitivity to external noise disturbances since both beams have the same optical path, a simple configuration that is easy to realize with all-fiber components, no dependence on polarization state of the input light. From relation (1), the birefringence (B) of the PM fiber is calculated by measuring the wavelength spacing between two consecutive transmission dips ($\Delta\lambda$) and the fiber length (L) with the following relation [16]:

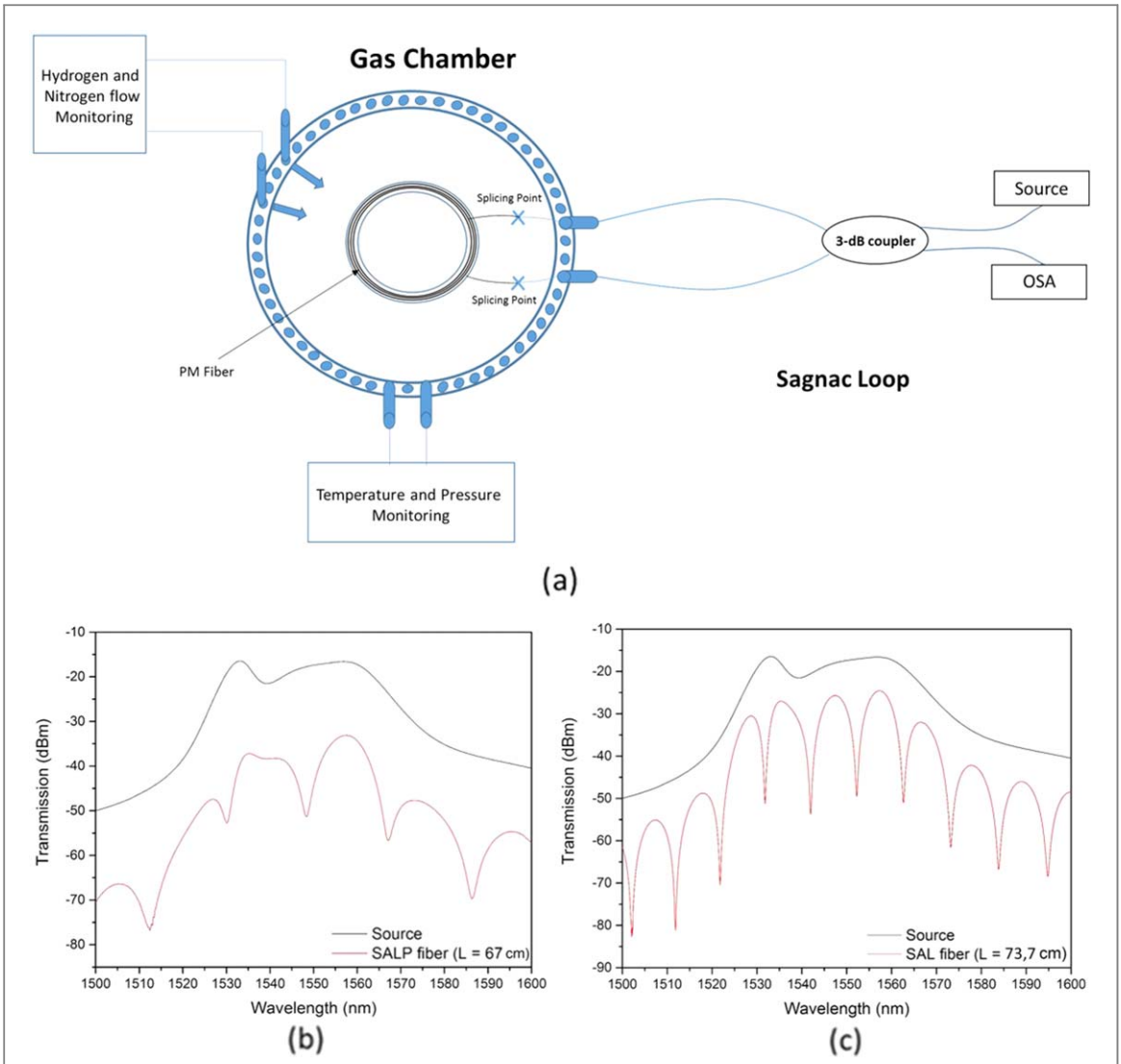

Figure 3. (a) Schematic of the hydrogenation setup. (b) Transmission spectra of the interferometer with SALP fiber with a length of 67 cm inside the FLM. (c) Transmission spectra of the interferometer with SAL fiber with a length of 73.7 cm inside the FLM.

$$B = \frac{\lambda^2}{L\,\Delta\lambda}, \tag{2}$$

where λ is the central wavelength (between two dips).

The dip wavelengths λ occur when $T = 0$, so that:

$$\lambda = \frac{BL}{q} \tag{3}$$

leading to:

$$\frac{\lambda - \lambda_0}{\lambda_0} = \frac{\Delta B}{B_0}, \tag{4}$$

where q is an integer, B_0 and λ_0 the intial birefringence and wavelength of dip, and, $\Delta B = B - B_0$ the birefringence variation due to external perturbations such as temperature T and pressure P. These relations demonstrate that the relative wavelength sifth ($[\lambda - \lambda 0]/\lambda 0$) is independent to the fiber length and to the value of the initial wavelength (λ_0). These behaviors are observable on the figures 4(a) and (b). The evolution of transmission spectrum of a FLM is identical for each transmission dip.

The transmission spectra of the FLM composed of 67 cm long length of SALP-fiber and of 73.7 cm long length of SAL-fiber are shown in figures 3(b) and (c), respectively. The mean birefringence of the SALP-fiber is about of $1.9 \times 10^{-4} \pm 0.1 \times 10^{-4}$ and about $3.1 \times 10^{-4} \pm 0.1 \times 10^{-4}$ for the SAL-fiber. These values were obtained by averaging the B values calculated for each $\Delta\lambda$ of the spectra in figures 3(b) and (c). As demonstrated

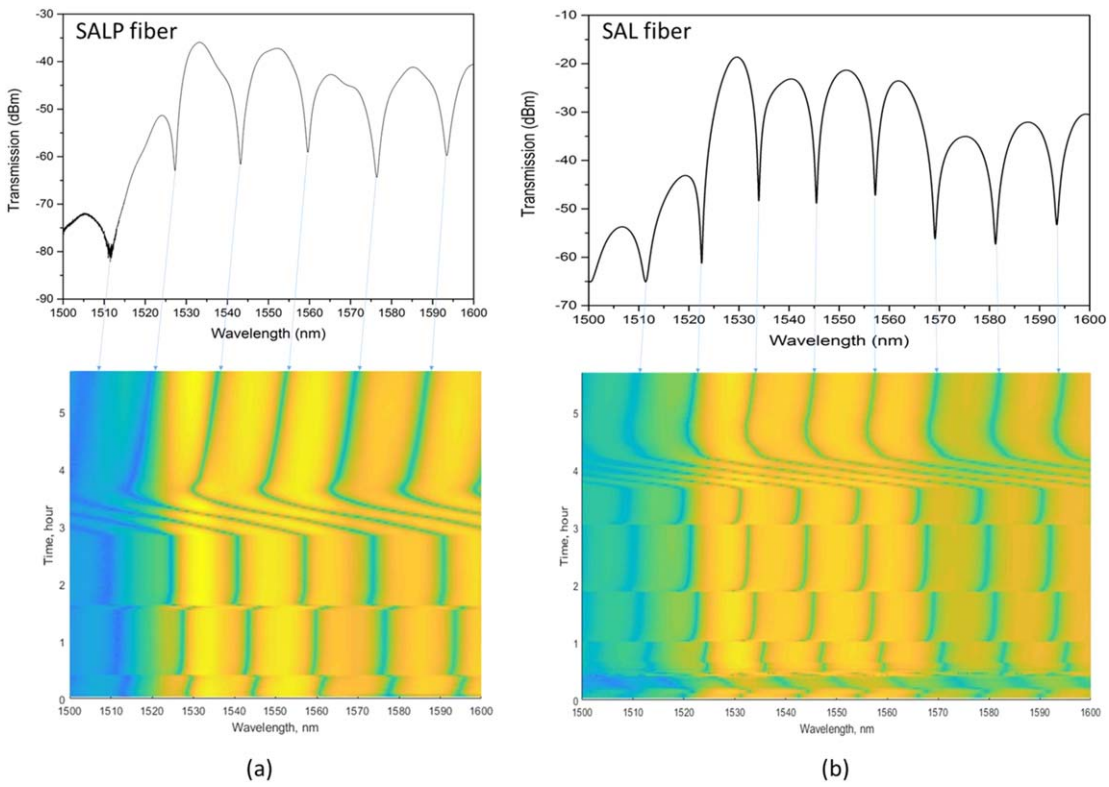

Figure 4. Spectrum shifts during N_2-gas pressure and temperature sensitivity tests for the: (a) SALP optical fiber, (b) SAL optical fiber.

in [14], it is worth noticing that the birefringence is only induced by the SAP, since a similar fiber with empty SAPs (air holes) does not exhibit a measurable birefringence.

3.2. Hydrogenation bench for in-line measurements

We have specially developed a gas chamber for studying in real-time the impact of H_2 gas (or other gas) on the optical properties of fiber samples. The chamber contains two channels for H_2 gas and nitrogen (N_2) gas flowing with controlled pressure and temperature. Four hermitic optical connectors enable to connect optical fibers or fiber-components inside the chamber to the interrogation setup for on-line measurements and dynamic comparisons between fiber samples or fiber-components. As illustrated in figure 3(a), the PM fiber under-test is inserted into the chamber and connected to the fiber-coupler of the FLM for enabling on-line measurement of the birefringence variation under H_2 gas.

Before investigating the impact of H_2 gas on the SALP-fiber, we have measured its sensitivity to the N_2-gas pressure and to the temperature. SALP-fiber and SAL-fiber were both inserted in the chamber and connected to an FLM for comparing their sensitivities. The sensitivity to N_2-gas pressure was studied by increasing the pressure of the gas into the chamber from 0 to 60 bar by steps of 20 bar. The temperature was set at 16 °C. As expected, the variation of the pressure yields a modification of the birefringence of both fibers leading to an evolution of the transmitted spectrum of each FLM (figures 4(a) and (b)). The variation of the birefringence (ΔB) induces a shift of the dip wavelengths λ and a modification of the spacing ($\Delta\lambda$) between each dips accordingly to ΔB. As shown theoretically in relation (3) and experimentally in figures 4(a) and (b), the spectral shift of a dip of the FLM spectrum is a relevant measure of the sensitivity of a PM fiber to the physical parameter considered. In the FLM configuration, the shift of a dip is only yielded by ΔB, independently to the length of the PM fiber, enabling direct comparison between different PM fibers without considering their length. It worth noticing that the length of the PM fiber affects only the bandwidth of the dips, which one could influence the uncertainty of the dip wavelength measurement.

As shown in figures 4(a) and 5(a), the transmission spectrum of the FLM shifts toward lower wavelengths when the pressure is increased. By measuring the wavelength shift of a dip for each pressure, we have calculated for the SALP fiber a wavelength dependency of -0.098 ± 0.03 nm bar^{-1}, and a pressure sensitivity $S_p = (1/\lambda_0)(d\lambda/dP)$ of -6.2×10^{-5}/bar with $\lambda_0 = 1558.25$ nm the initial dip wavelength (at $P = 0$ bar). For the SAL-fiber, we have calculated a wavelength dependency of -0.064 ± 0.04 nm bar^{-1} and a pressure sensitivity

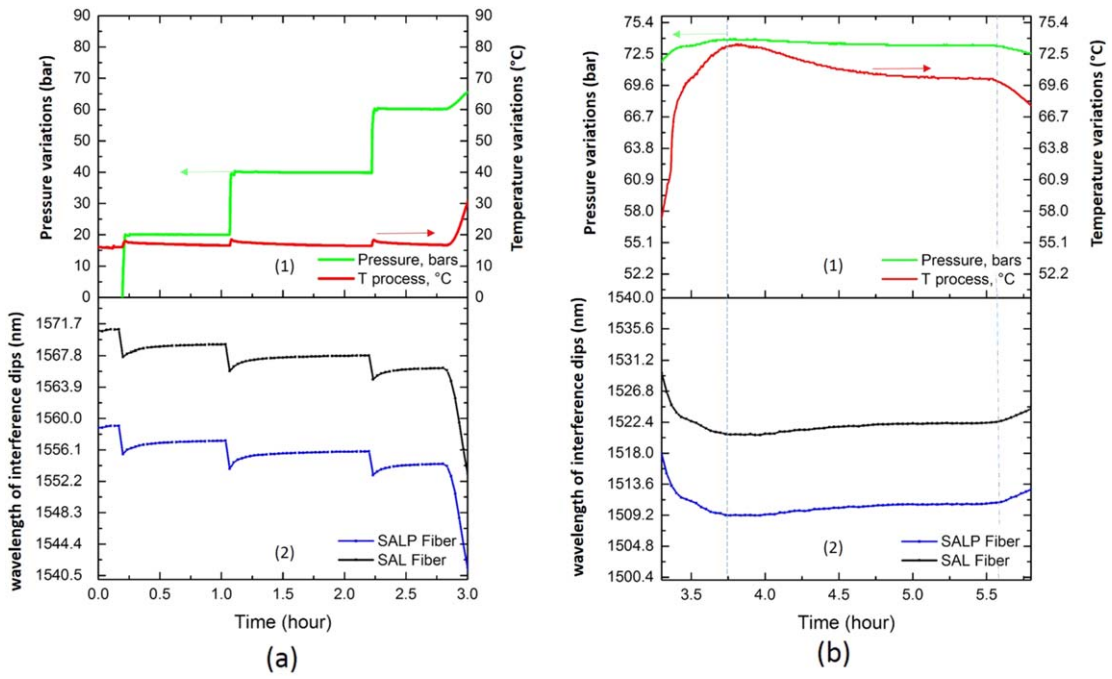

Figure 5. a(1) Pressure and Temperature variations for the pressure sensitivity test. a(2) Interference spectrum shift of the SAL (black curve) and SALP (blue curve) fiber. b(1) Pressure and temperature variations for the temperature sensitivity test. b(2) Interference spectrum shift of the SAL (black curve) and SALP (blue curve) fiber.

$S_p = -4.1 \times 10^{-5}/\text{bar}^{-1}$ with $\lambda_0 = 1570.8$ nm. The wavelength shifts were measured when the temperature measured in the chamber ($T_{process}$) is stabilized, after the introduction of additional N_2 gas.

The sensitivity to the temperature was measured at an N_2 pressure of 72.5 bar by decreasing the temperature from 72.5 °C to 69.6 °C leading to a shift of the transmission spectrum toward longer wavelengths (figure 5(b)). By linearly fitting the wavelength shift of a dip, we have calculated for the SALP fiber a wavelength dependency of -0.52 ± 0.05 nm °C^{-1}, and a temperature sensitivity $S_T = (1/\lambda_0)(d\lambda/dT)$ of -3.4×10^{-4} °C^{-1} with $\lambda_0 = 1522.54$ nm. For the SAL-fiber, we have calculated a wavelength dependency of -0.53 ± 0.02 nm °C^{-1} and a temperature sensitivity $S_T = -3.5 \times 10^{-4}$ °C^{-1} with $\lambda_0 = 1511.18$ nm.

Both FLMs are sensitive to N_2-gas pressure and the temperature variations confirming the interests of PM-fiber based FLM configurations for sensing applications [17]. Both fibers have the same temperature sensitivity (S_T) and a similar pressure sensitivity (S_p) that is more than 5 times smaller than S_T. These measurements demonstrate that Pd particles embedded in SAPs do not have a significant effect on the birefringence variations under pressure and/or temperature variations, and hence they will not induce parasitic variations on the birefringence (or wavelength dip) measurements during the diffusion of H_2 gas into the fiber (at constant pressure and temperature).

4. Hydrogen sensing: experimental results and analysis

In order to evaluate the contribution of Pd particles embedded into an optical fiber for the detection of H_2, both fiber samples (SALP and SAL) were inserted in the chamber and connected to FLMs for comparing their sensitivities. The chamber was initially filled during few hours with N_2 gas ($P = 20$ bar at room temperature) to check the hermiticity of the chamber. N_2 gas is then evacuated and replaced by the H_2 gas with a pressure of 60 bar (figure 6). To accelerate the diffusion kinetics of H_2 in the optical fiber, the temperature of the autoclave is increased to 70 °C. It is worth noticing that this temperature is in agreement with the repository conditions of radioactive wastes where the temperature could reach 90 °C in the repository cells for long-lived and high-level wastes. The pressure of H_2 and temperature are kept constant during 123 h for enabling dynamic measures during the diffusion of H_2 into the fibers. The gas is finally released and the temperature dropped down to room temperature.

When both fibers are exposed to H_2 gas, the FLM spectra shift toward longer wavelengths (figure 7(a) and (b)). The dynamic of the wavelength shift of one dip of the spectrum is plotted in figure 7(c) for both fibers. These curves have been obtained by measuring the transmission spectrum of both FLMs each 2 min Both curves are plotted from 3.5 to 126.5 h for presenting only the impact of diffusion of H_2 gas into the fibers. The variations of

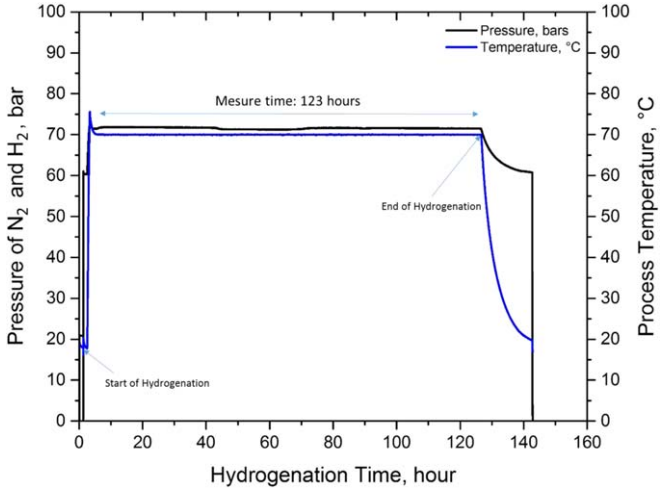

Figure 6. Hydrogenation protocol of the SAL and SALP optical fibers.

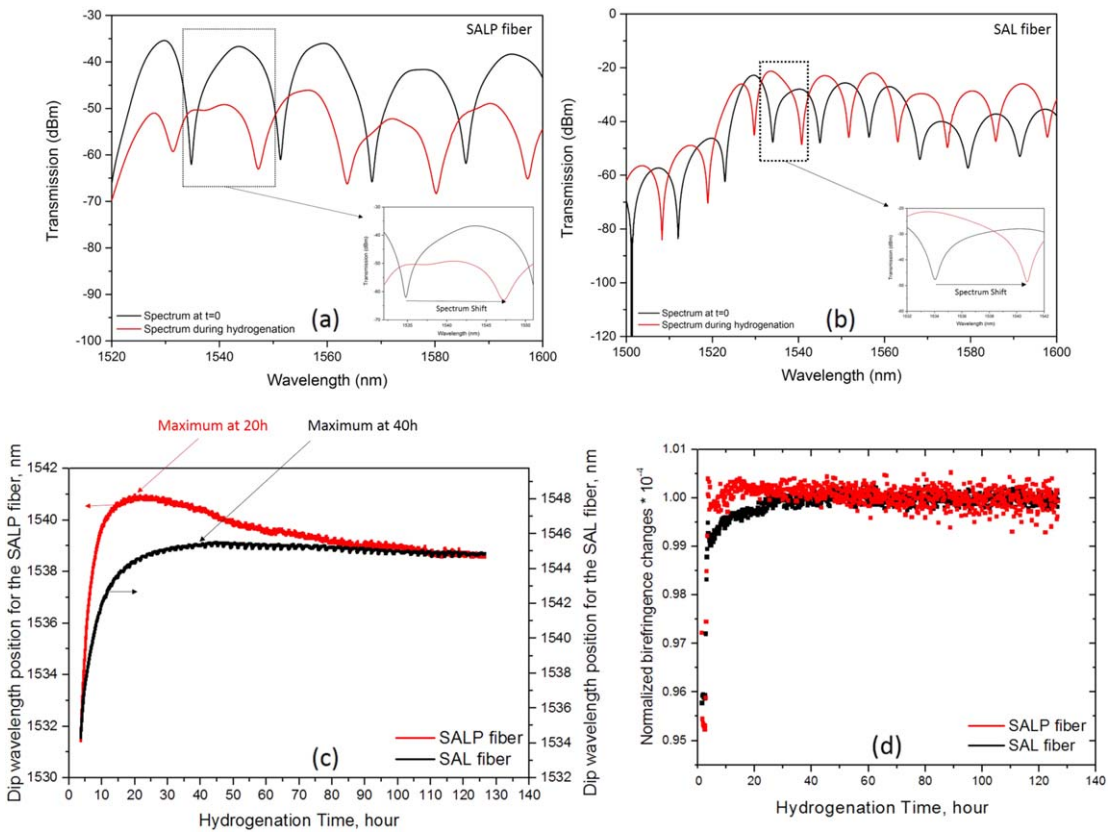

Figure 7. The FLM spectra shift during hydrogenation of a (a) PANDA SALP optical fiber, (b) PANDA SAL optical fiber. (c) Wavelength shift of an interference dip of a PANDA SALP optical fiber (Red curve) and of a PANDA SAL optical fiber (Black curve) during hydrogenation. (d) Normalized birefringence changes ($B/B_{saturation}$) a PANDA SALP optical fiber (Red curve) and of a PANDA SAL optical fiber (Black curve) during hydrogenation.

temperature and pressure yielded when H_2 gas is introduced in the chamber are not presented. The diffusion of H_2 gas induces a shift of the dips to longer wavelengths for both fibers, until a stabilization of the dip wavelengths corresponding to the saturation of H_2 diffusion into the fiber core. More precisely, the shift of the dip wavelength reaches a maximum before its stabilization. As shown in figure 7(c) both curves have different behaviors. The maximum is reached after 20 h for the SALP-fiber, against 40 h for the SAL-fiber. Furthermore, at the maximum, the shift of wavelength dip of the SALP-fiber is 32% time larger than the shift at saturation, while it is

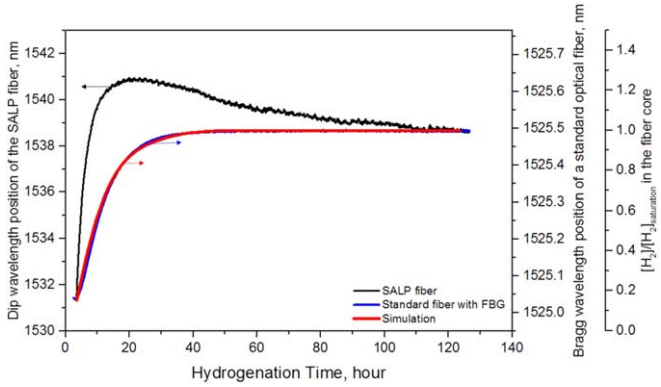

Figure 8. Wavelength shift of an interference dip of a PANDA SALP optical fiber (Black curve) and of a standard optical fiber with Bragg grating written inside the core (blue curve) during hydrogenation. Simulations of the evolution of the hydrogen concentration in the center of a 125 μm optical fiber (Red curve).

only 6% for the SAL-fiber. These results demonstrate that Pd particles embedded in the SAP enhance the impact of H_2 gas diffusion into the fiber on the birefringence properties.

The variation of the birefringence is then calculated by equation (3), figure 7(d) represents the normalized birefringence ($B/B_{\text{saturation}}$) for both fibers. These variations are similar to the ones of the dip wavelengths of both fibers. The SALP-fiber presents a stronger birefringence variation in comparison with the SAL-fiber, demonstrating the interests of the Pd particles.

In order to evaluate the detection performances of the SALP fiber, we inserted into the gas chamber, a standard optical fiber (SMF28) composed of a Bragg grating written inside the core of the fiber. The shift of the Bragg wavelength as a function of the H_2 diffusion time in the fiber is shown in blue in figure 8. We have also calculated, from an analytical model developed by Swart *et al* [18], the kinetic of H_2 diffusion into the core of a standard optical fiber (red curve). The evolution of the concentration of H_2 into the fiber core follows perfectly the shift of the Bragg wavelength. The diffusion of hydrogen into a standard silica-based singlemode fiber follows a cylindrical symmetry. Consequently, there is no induced birefringence but it yields a variation of the refractive index that can be captured by following the Bragg wavelength evolution of a fiber Bragg grating inscribed inside the core of the fiber. The evolution of the Bragg wavelength is thus representative of the variation of the concentration of H_2 into the fiber core. The comparison between the shift of the Bragg wavelength and the wavelength shift of an interference dip of the SALP fiber shows different dynamics. As shown in figure 8, the shift of the dip wavelength of SALP fiber exhibits a faster response time and a larger amplitude. It is shifted by about 9 nm after 20 h of hydrogen diffusion, while it is shifted by less than 1 nm for the standard optical fiber. This comparison emphasises furthermore the interest of the SALP-fiber for detecting slow leakage of H_2 gas with higher sensitivity and faster response time than the standard optical fiber.

These results demonstrate the impact of Pd particles embedded in the SAPs on the optical properties of the SALP-fiber that are induced by the modifications of the strain field pattern (generated by the SAPs) during the diffusion of H_2 gas into the fiber. Nevertheless, it would be interesting to study, the interplays between the variation of the strain field pattern during the diffusion of H_2 gas and the diffusion kinetic of the gas into the SAPs composed or not of embedded Pd particles for both polarization axes of the fiber. This study might explain the faster response time of the SALP-fiber and even the SAL-fiber than the standard optical fiber, and also the maximum of the dip wavelength shift that is much higher for the SALP-fiber.

5. Conclusion

We have fabricated two disruptive birefringence optical fibers composed of two stress applying parts of SAL glass material with or without embedded Palladium particles. We have characterized these fibers and reported the first experimental study of the evolution of their birefringence during the diffusion of H_2 gas into the fiber by inserting the fiber within a fiber loop mirror interferometer (FLM) associated with a specially developed gas chamber. On-line measurement dynamics and comparisons with the fiber without Pd particles demonstrate the contribution of Pd particles resulting in a faster response time. The maximum shift of the dip wavelengths (i.e. birefringence variation) of the FLM interferometer is reached after 20 h of hydrogenation (at 70 °C and 60 bar) while it requires 40 h for the reference fiber (SAL-fiber) and around 50 h for a standard optical fiber. These results pave the way to the realization of robust optical fiber with enhanced sensitivity to H_2 gas for developing

sensing systems compatible with long-term hydrogen monitoring applications in extreme and harsh environments, such as radioactive waste repositories.

Acknowledgments

The authors acknowledge financial support from the European project Modern2020, Euratom research and training program 2014–2018 under grant agreement No 662177. Also, the authors would like to thank the French National Radioactive Waste Management Agency (ANDRA) for their financial support.

ORCID iDs

Georges Humbert https://orcid.org/0000-0002-4910-0569

References

[1] Cashdollar K L, Zlochower I A, Green G M, Thomas R A and Hertzberg M 2000 Flammability of Methan, propane, and hydrogengases *J. Loss Prev. Process Ind.* **13** 327–40
[2] Yang M, Yang Z, Dai J and Zhang D 2012 Fiber optic hydrogen sensors with sol-gel WO_3 coatings *Sensors Actuators* B **166-7** 632–6
[3] Huiberts J N, Griessen R, Rector J H, Wijngaarden R J, Dekker J P, De Groot D G and Koeman N J 1996 Yttrium and lanthanum hydride films with switchable optical properties *Nature* **380** 231–4
[4] Butler M A 1984 Optical fiber hydrogen sensor *Appl. Phys. Lett.* **45** 1007–9
[5] Monzon-Hernandez D, Luna-Moreno D and Martinez-Escobar D 2009 Fast response fiber optic hydrogen sensor based on palladium and gold nano-layers *Sensors Actuators* B **136** 562–6
[6] Tabib-Azar M, Sutapun B, Petrick R and Kazemi A 1999 Highly sensitive hydrogen sensors using palladium coated fiber optics with exposed cores and evanescent field interactions *Sensors Actuators* B **56** 158–63
[7] Villatoro J and Monzon-Hernandez D 2005 Fast detection of hydrogen with nano fiber tapers coated with ultra thin palladium layers *Opt. Express* **13** 5087–93
[8] Caucheteur C, Debliquy M, Lahem D and Mégret P 2008 Hybrid fiber gratings coated with a catalytic sensitive layer for hydrogen sensing in air *Opt. Express* **16** 16854
[9] Caucheteur C, Debliquy M, Lahem D and Mégret P 2008 Catalytic fiber Bragg grating sensor for hydrogen leak detection in air *IEEE Photonics Technol. Lett.* **20** 96–8
[10] Yang M, Sun Y, Zhang D and Jiang D 2010 Using Pd/WO_3 composite thin films as sensing materials for optical fiber hydrogen sensors *Sensors Actuators* B **143** 750–3
[11] Greco F, Ventrelli L, Dario P, Mazzolai B and Mattoli V 2012 Micro-wrinkled palladium surface for hydrogen sensing and switched detection of lower flammability limit *Int. J. Hydrog. Energy* **37** 17529–39
[12] Farrow J *et al* 2019 Monitoring parameter screening: test cases *Modern 2020 Project Deliverable D2.2*
[13] Leparmentier S, Auguste J L, Humbert G, Delaizir G and Delepine-Lesoille S 2015 Fabrication of optical fibers with palladium metallic particles embedded into the silica cladding *Opt. Mater. Express* **5** 2578–86
[14] Kudinova M, Humbert G, Auguste J L and Delaizir G 2017 Multimaterial polarization maintaining optical fibers fabricated with the powder-in-tube technology *Opt. Mater. Express* **7** 3780–90
[15] Auguste J L, Humbert G, Leparmentier S, Kudinova M, Martin P O, Delaizir G, Schuster K and Litzkendorf D 2014 Modified Powder-in-Tube technique based on … processing of powder materials for fabricating specialty optical fibers *Materials* **7** 6045–63
[16] Kim D-H and Kang J U 2004 Sagnac loop interferometer based on polarization maintaining photonic crystal fiber with reduced temperature sensitivity *Opt. Express* **12** 4490
[17] Liu Y, Liu B, Feng X, Zhang W, Zhou G, Yuan S, Kai G and Dong X 2005 High-birefringence fiber loop mirrors and their applications as sensors *Appl. Opt.* **44** 2382–90
[18] Swart P L and Chtcherbakov A A 2002 Study of hydrogen diffusion in Boron/Germanium codoped optical fiber *J. Lightwave Technol.* **20** 1933–41